Spectral and temporal structures of high-order harmonic generation of Na in intense mid-ir laser fields

Xi Chu and Shih-I Chu
Department of Chemistry, University of Kansas, and Kansas Center for Advanced Scientific Computing, Lawrence, Kansas 66045

Cecil Laughlin
School of Mathematical Sciences, University of Nottingham, Nottingham NG7 2RD, England
(Received 6 December 2000; published 5 June 2001)

We present a three-dimensional quantum study of high-order harmonic generation (HHG) of the Na atom in intense mid-ir laser fields. An accurate one-electron model potential is constructed for the description of the Na atom. The time-dependent Schrödinger equation is solved by means of the *time-dependent generalized pseudospectral method*, allowing *nonuniform* and optimal spatial grid discretization and accurate and efficient propagation of the wave function in space and time. Excellent agreement of the HHG spectrum in the length and acceleration forms is obtained from the lowest harmonics up to the cutoff. The HHG power spectrum shows fine structures and significant enhancement of the intensities of the lower harmonics due to the strong coupling of the $3s$-np states and the $3s$-$3p$ multiphoton resonance. We use a wavelet transform to present a detailed time-frequency analysis of the whole range of the HHG power spectrum. The results reveal striking details of the spectral and temporal fine structures of HHG, providing insights into different HHG mechanisms in different energy regimes of Na atoms at long wavelengths.

DOI: 10.1103/PhysRevA.64.013406 PACS number(s): 32.80.Rm, 42.65.Ky, 32.80.Wr, 42.50.Hz

I. INTRODUCTION

The study of the interaction of atoms and molecules with intense laser fields is a subject of much current interest in science and technology. Several novel nonlinear optical phenomena have been observed, including multiple high-order harmonic generation (HHG) [1,2], the main focus of this paper. Most of the experimental and theoretical studies of HHG so far have been carried out with short laser pulses in the near-visible or UV regime [1,2]. The generation of harmonics in rare-gas atoms that extend up to orders of about 300 (well within the water window region) has been recently reported [2]. However, the experimental progress in such a table-top soft x-ray light source is partially limited by the lack of appropriate materials for the measurement of vuv or XUV pulse lengths. Recently, it has been suggested [3,4] that an intense mid-infrared (ir) laser light source may be used to generate HHG in the visible to UV regime, allowing the application of frequency resolved optical grating [5] for the full characterization of the harmonic's amplitude and phase. The advent of mid-ir laser technology [3] opens the possibility of studying multiphoton processes in systems with lower binding energies (such as alkali atoms) than those previously studied (such as rare-gas and H atoms), allowing the exploration of fundamentally different strong-field phenomena at longer wavelengths. Motivated by such recent advances, we present in this paper a precise three-dimensional (3D) calculation and theoretical analysis of the HHG process in a Na atom driven by intense mid-ir laser pulses. The study reveals detailed spectral and temporal fine structures, as well as new insights into HHG mechanisms in different energy regimes.

In the present study, we first construct an accurate one-electron model potential for the description of the Na atom that reproduces both the experimental energy levels and oscillator strengths. The time-dependent Schrödinger equation is solved numerically by means of the *time-dependent generalized pseudospectral* (TDGPS) method recently developed [6]. As demonstrated in recent works [6–11], the TDGPS method allows for *nonuniform* and optimal spatial grid discretization and efficient and accurate time propagation. The method has been applied successfully in an *ab initio* study of HHG of atomic H [6,7] and in (self-interaction-free) *time-dependent density functional theoretical* (TDDFT) studies of rare-gas atoms [8,9] and molecules [10] in intense laser fields. The TDGPS method has been also recently applied to the calculation of high-resolution spectroscopy of 3D Rydberg atoms in external fields with results in agreement with experimental spectra line by line, well above the classical Stark saddle point and classically chaotic regimes [11]. In this paper, we perform a time-frequency analysis of the HHG spectrum by means of the wavelet transform [7,12].

The paper is organized as follows. In Sec. II, we present details of the Na one-electron model potential used in the current study. The TDGPS procedure for the calculation of the HHG spectrum is then outlined in Sec. III. Detailed discussion of the results and analysis of the wavelet time-frequency spectrum in different energy regimes is presented in Sec. IV. This is followed by a conclusion.

II. ANGULAR-MOMENTUM-DEPENDENT MODEL POTENTIAL FOR NA

Model potential methods [13] have been widely used to provide accurate descriptions of electron scattering [14,15], photoionization [16,17], and particle impact ionization [18,19] processes, as well as for the calculation of atomic and molecular properties [20–22] for one- and two-valence electron systems. A feature of these calculations is that the model potential describing the valence-electron–core interaction is chosen to have the correct long-range polarization

TABLE I. Model potential parameters for Na (in a.u.)

l	α	r_c	S	A_1	A_2	B_1	B_2
0	0.946	2.05	3.4776465	−4.4987218	−0.77850759	2.54	1.27
$\geqslant 1$	0.946	2.05	1.6341570	−6.7354384	−0.23873675	1.88	0.94

terms, and the parameters that determine the short-range part of the potential are chosen so that the experimental spectra and low-energy electron scattering phase shifts are reproduced to very high accuracy for all angular-momentum symmetries. The angular-momentum-dependent model potential we constructed for Na has the following form:

$$V_l = -\frac{\alpha}{2r^4} W_6\left(\frac{r}{r_c}\right) - \frac{1}{r} - \left(\frac{N-S}{r} + A_1\right) e^{-B_1 r} - \left(\frac{S}{r} + A_2\right) e^{-B_2 r}, \quad (1)$$

where α is the Na^+ core dipole polarizability [23], W_n is a core cutoff function given by

$$W_n(x) = 1 - \left[1 + nx + \frac{(nx)^2}{2!} + \cdots + \frac{(nx)^n}{n!}\right] e^{-nx} \quad (2)$$

and r_c is an effective Na^+ core radius. In the present work we find it is sufficient to use two different angular-momentum-dependent model potentials, one for states with $l=0$ and another for states with $l \geqslant 1$. The values of the parameters determined are listed in Table I. Table II presents a comparison of the bound-state energies predicted by the model potentials and the experimental values. Agreement is satisfactory in all cases. Further, the lifetime of the Na $3p$ state is calculated to be 16.14 ns, in very good agreement with the latest measured values, 16.27(6) [24] and 16.230(16) ns [25], deduced from the observed spectra of Na_2 vibrational levels formed by photoassociation of ultracold Na atoms.

III. TIME-DEPENDENT GENERALIZED PSEUDOSPECTRAL METHOD

We consider the solution of the time-dependent Schrödinger equation for a Na atom in linearly polarized (LP) mid-ir pulsed laser fields, in atomic units,

$$i\frac{\partial}{\partial t}\psi(\mathbf{r},t) = \hat{H}\psi(\mathbf{r},t) = [H_0(\mathbf{r}) + \hat{v}(\mathbf{r},t)]\psi(\mathbf{r},t). \quad (3)$$

Here H_0 is the field-free Hamiltonian for the Na atom,

$$H_0 = -\frac{1}{2}\nabla^2 + \sum_l |Y_l^0\rangle V_l \langle Y_l^0|, \quad (4)$$

where V_l is the model potential described in Eq. (1) and Y_l^0 is a spherical harmonic. The atom-field coupling is given by

$$\hat{v}(\mathbf{r},t) = -\mathbf{E}\cdot\mathbf{r} f(t)\sin\omega t = -Ezf(t)\sin\omega t, \quad (5)$$

where $\mathbf{E}(\|\hat{\mathbf{z}})$ is the electric field, ω is the laser frequency, and $f(t)$ is the laser pulse shape (a $\sin^2$ pulse shape is used). The propagation of the wave function is performed by means of the *time-dependent generalized pseudospectral* method [6]. The radial coordinate r is discretized by use of *generalized pseudospectral* techniques [26,27], allowing *nonuniform*

TABLE II. Comparison of the calculated Na energies with the experimental values (in a.u.). For each angular momentum l, two rows of energies $E(n,l)$ are listed: the upper row refers to the calculated model-potential energies, and the lower row refers to the experimental values.

	$E(n,l)$							
$l\backslash n$	3	4	5	6	7	8	9	10
0	−0.1888621	−0.0715793	−0.0375849	−0.0231323	−0.0156623	−0.0113043	−0.0085415	−0.0066806
	−0.1888621	−0.0715792	−0.0375850	−0.0231322	−0.0156623	−0.0113042	−0.0085415	−0.0066805
1	−0.1115498	−0.0509354	−0.0291959	−0.0189202	−0.0132542	−0.0098003	−0.0075390	−0.0059805
	−0.1115500	−0.0509352	−0.0291950	−0.0189195	−0.0132536	−0.0097998	−0.0075391	−0.0059790
2	−0.0559387	−0.0314419	−0.0201051	−0.0139517	−0.0102444	−0.0078399	−0.0061922	−0.0050142
	−0.0559375	−0.0314426	−0.0201061	−0.0139526	−0.0102452	−0.0078405	−0.0061928	−0.0050149
3		−0.0312681	−0.0200107	−0.0138956	−0.0102085	−0.0078155	−0.0061750	−0.0050016
		−0.0312685	−0.0200109	−0.0138956	−0.0102085	−0.0078156	−0.0061751	−0.0050015
4			−0.0200023	−0.0138904	−0.0102051	−0.0078132	−0.0061733	−0.0050004
			−0.0200024	−0.0138904	−0.0102051	−0.0078132	−0.0061733	−0.0050004

and optimal grid discretization: a denser mesh near the origin and a sparser mesh for the outer regions. This *nonuniform* grid discretization is essential, since it allows accurate treatment of the physically most significant short-range region and, at the same time, it takes into account the long-range nature of the Coulomb interaction. The number of grid points needed to achieve convergence is modest, often orders of magnitude smaller than those used in conventional equal-spacing discretization methods [26]. For example, the use of 20 radial grid points is sufficient to achieve the first few (field-free) Na eigenvalues to 10–14 digits of accuracy.

The time propagation of the wave function is achieved by the second-order split-order method in the *energy* representation [6]

$$\psi(t+\Delta t)=e^{-iH_0\Delta t/2}\exp[-iv(t+\Delta t/2)\Delta t]e^{-iH_0\Delta t/2}\psi(t)+O(\Delta t^3). \tag{6}$$

Use of the *energy* representation, which is different from conventional split-order techniques using a coordinate-momentum representation [28,29], eliminates undesirable *high-energy* components and allows considerably larger time steps Δt to be employed. Further, as shown in [6], each partial-wave wave function can be propagated *independently* since H_0 is diagonal in the *energy* representation and $\hat{v}(t)$ is diagonal in the coordinate representation. Since $e^{-iH_0\Delta t/2}\exp[-iv(t+\Delta t/2)\Delta t]e^{-iH_0\Delta t/2}$ is unitary, the normalization of the wave function is automatically preserved by Eq. (6) and we have checked that the norm of the field-free time-dependent wave function is preserved to at least ten digits of accuracy during the whole time propagation. As demonstrated in recent studies of both strong-field HHG processes [6–10] and Rydberg-atom high-resolution spectroscopy [11], the TDGPS procedure is computationally more efficient and accurate than the conventional time-dependent techniques using *equal-spacing* grid discretization. A highly accurate time-dependent wave function is essential to the present study of the spectral and temporal fine structures of HHG. The quality of the time-dependent wave function obtained by the TDGPS method is demonstrated by the excellent agreement of the whole HHG power spectra in the length and acceleration forms (from the lowest harmonics to the cutoff) in the present and other recent TDGPS calculations [6–10].

Once the time-dependent wave function is available, one can calculate the expectation value of the induced dipole moment in the *length* form,

$$d_L(t)=\langle\psi(\mathbf{r},t)|z|\psi(\mathbf{r},t)\rangle. \tag{7}$$

The induced dipole in the acceleration form can also be determined. By taking into account the special structure of the model potential, Eq. (1), the following expression for the expectation value of the *dipole acceleration* form is obtained:

$$\begin{aligned}d_A(t)&=\frac{\partial^2}{\partial t^2}\langle\psi(\mathbf{r},t)|z|\psi(\mathbf{r},t)\rangle=\langle\psi(\mathbf{r},t)|(H,[H,z])|\psi(\mathbf{r},t)\rangle\\&=\frac{1}{2\sqrt{3}}\langle R_0|\nabla^2V_0r|R_1\rangle+\frac{1}{2\sqrt{3}}\langle R_1|rV_0\nabla^2|R_0\rangle\\&\quad-\frac{1}{2\sqrt{3}}\langle R_1|\nabla^2rV_0|R_0\rangle-\frac{1}{2\sqrt{3}}\langle R_0|V_0r\nabla^2|R_1\rangle\\&\quad+\frac{1}{\sqrt{3}}\left\langle R_1\left|\frac{V_0}{r}\right|R_0\right\rangle+\sqrt{3}\left\langle R_0\left|\frac{V_0}{r}\right|R_1\right\rangle\\&\quad-\frac{1}{\sqrt{3}}\langle R_0|V_0^2r|R_1\rangle-\frac{1}{\sqrt{3}}\langle R_1|rV_0^2|R_0\rangle\\&\quad+\frac{1}{\sqrt{3}}\left\langle R_0\left|V_0\frac{\partial}{\partial r}\right|R_1\right\rangle-\frac{1}{\sqrt{3}}\left\langle R_1\left|\frac{\partial}{\partial r}V_0\right|R_0\right\rangle\\&\quad-\left\langle\psi(\mathbf{r},t)\left|\frac{\partial}{\partial z}V_1\right|\psi(\mathbf{r},t)\right\rangle,\end{aligned} \tag{8}$$

where

$$R_l\equiv R_l(r,t)=\langle Y_l^0(\theta,\phi)|\psi(\mathbf{r},t)\rangle. \tag{9}$$

Finally, by performing the Fourier transform of $d_L(t)$ and $d_A(t)$, we obtain the HHG power spectrum in the length and acceleration forms, respectively,

$$d_L(\omega)=\frac{1}{t_f-t_i}\int_{t_i}^{t_f}d_L(t)e^{-i\omega t}dt, \tag{10}$$

$$d_A(\omega)=\frac{1}{(t_f-t_i)\omega^2}\int_{t_i}^{t_f}d_A(t)e^{-i\omega t}dt. \tag{11}$$

IV. RESULTS AND DISCUSSION

In this section we discuss some results of HHG calculations for the Na atom in mid-ir laser pulsed fields. First we start by examining the differences between the nonlinear response behaviors of alkali Na and H atoms, both of which have one active valence electron. Then we carry out a detailed wavelet time-frequency analysis of the HHG power spectrum of Na and explore the different mechanisms responsible for the production of high harmonics in different energy regimes.

A. Comparison of the HHG power spectrum of Na and H atoms

Figure 1 shows the comparison of the HHG power spectrum of atomic H and Na at the same Keldysh parameter γ value [30], where $\gamma=\sqrt{I_p/2U_p}$, $U_p=E^2/4\omega^2$ is the ponderomotive energy, I the laser intensity, ω the laser frequency, and I_p the field-free ionization potential. γ is a qualitative indicator of the relative importance of multiphoton and *tunneling* mechanisms. For $\gamma<1$, the process is generally dominated by the tunneling mechanism, while the *multiphoton*

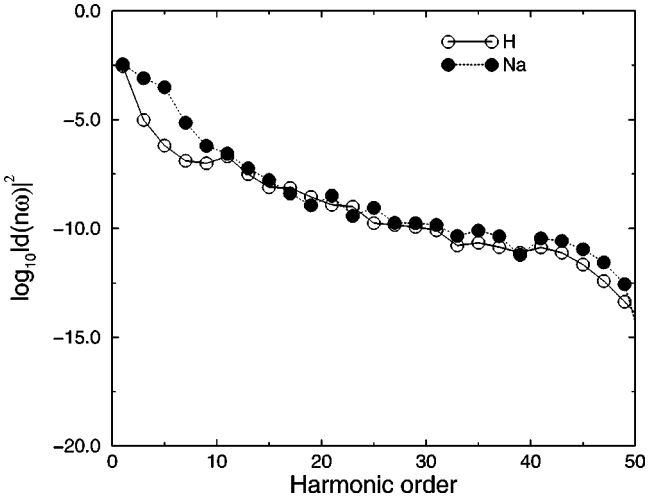

FIG. 1. Comparison of the HHG power spectrum of H and Na atoms with the same Keldysh parameter, $\gamma=0.8$. The laser intensity and wavelength used are 10^{14} W/cm^2 and 1064 nm, respectively, for H and 5.388×10^{12} W/cm^2 and 2817.8 nm, respectively, for Na. For both cases, it takes about 12 photons to ionize the electron. The laser used has a $\sin^2$ pulse shape and a duration of 20 optical cycles.

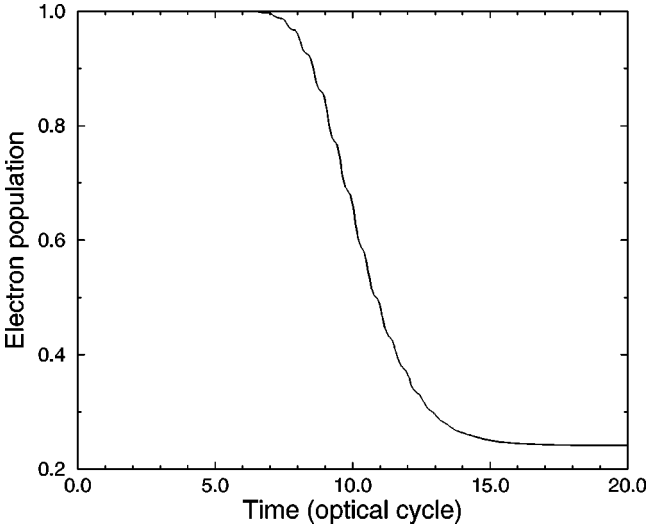

FIG. 2. The population of the ground state of Na as a function of time. The laser parameters used are the same as those in Fig. 1.

mechanism prevails when $\gamma>1$. For the HHG processes dominated by the tunneling mechanism, the cutoff harmonic position can be predicted by the quasiclassical two-step model [33,34], namely, $n_{cutoff}\simeq(I_p+3.17U_p)/\omega$. For atomic H irradiated by laser pulses with wavelength 1064 nm and intensity 10^{14} W/cm^2, the Keldysh parameter γ has the value of 0.8. The corresponding laser parameters for Na are wavelength 2,818 nm (in the mid-ir region) or 0.016 17 a.u. in frequency, and 5.388×10^{12} W/cm^2 in laser intensity. In both cases, it takes about 12 photon energies to ionize the atom. Figure 1 shows that the HHG power spectrum patterns for atomic H and Na atoms are rather similar with the notable exception of the lower harmonics, where the harmonic intensities for Na are several orders of magnitude larger than those of atomic H. Some enhancement is also visible in the cutoff region for Na. The significant enhancement of the Na lower harmonics can be attributed to the strong coupling of the ground $3s$ state to the first-excited $3p$ state that is absent in the atomic H case. Similar enhancement predictions have been reported recently also by Sheehy *et al.* [3] and by Schafer *et al.* [4], who have calculated the HHG power spectra of alkali atoms using different model potentials and different time-dependent numerical techniques. In the present calculation (Fig. 1), the field-free $3p$-$3s$ energy spacing amounts to 4.78 photon energies. For the alkali Na atom, the laser intensity 5.388 TW/cm^2 used is a rather strong field (as shown by the significant ionization of Na in Fig. 2), and we notice that $H3$, $H5$, $H7$, and $H9$ harmonics of Na are all enhanced. We shall explore the effect of multiphoton resonance on the HHG production in more details in a later part of this section.

Figure 3 shows a comparison of the Na HHG power spectrum in the length and acceleration forms. The agreement is excellent from the lowest harmonics, through the plateau, to the cutoff region and spans nearly 18 orders of magnitude in intensity, indicating that the time-dependent wave function is fully converged. In this calculation, we have used 300 radial grid points, 30 partial waves, and an absorber [6] placed at a large r distance, typically 200 a.u., to filter out the ionizing wave packet. Several novel features of the Na HHG power spectrum are noticed: (a) the harmonics near the cutoff regime are characterized by structureless and somewhat broadened harmonic peaks; (b) for harmonics well below the cutoff but beyond the ionization threshold, that is in the midplateau regime, the most salient feature is the multiple-peak splitting pattern within each main harmonic peak. These fine structures are completely reproducible and contain essential information about the electron quantum dynamics and underlying mechanism. Similar distinct features have been reported for the case of atomic H [7]. However, the alkali Na atom possesses additional features, particularly in the multiphoton resonance regime, not shared by the atomic H or rare-gas atoms.

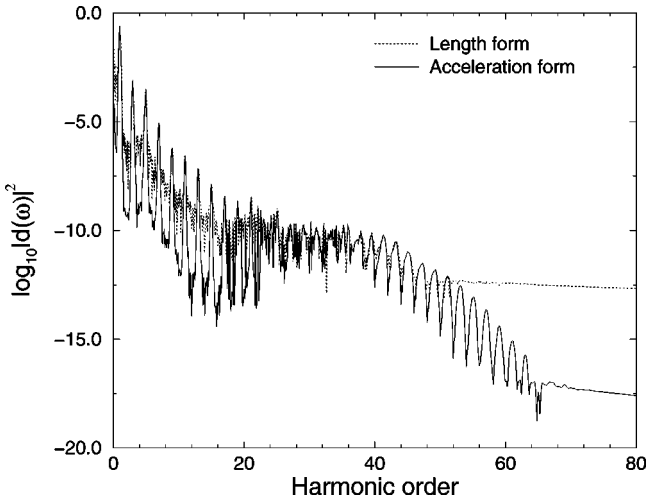

FIG. 3. Comparison of the HHG power spectrum of Na in the length and acceleration forms. Laser parameters same as those in Fig. 1.

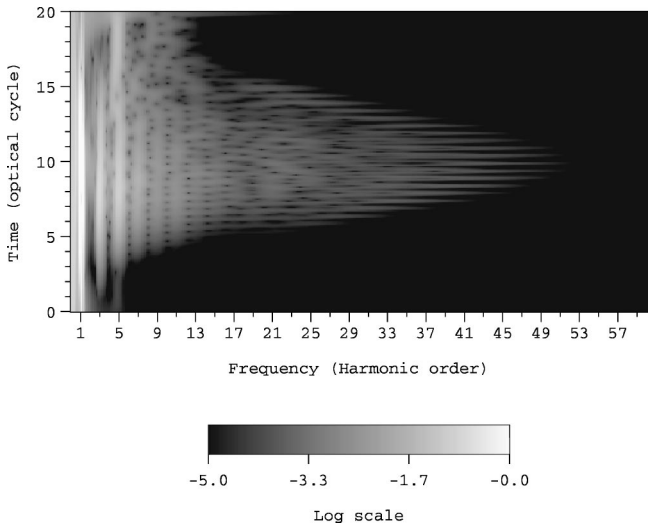

FIG. 4. The wavelet time-frequency spectrum (modulus) of atomic Na shown in the logarithmic scale (in powers of 10). Laser parameters are the same as those in Fig. 1.

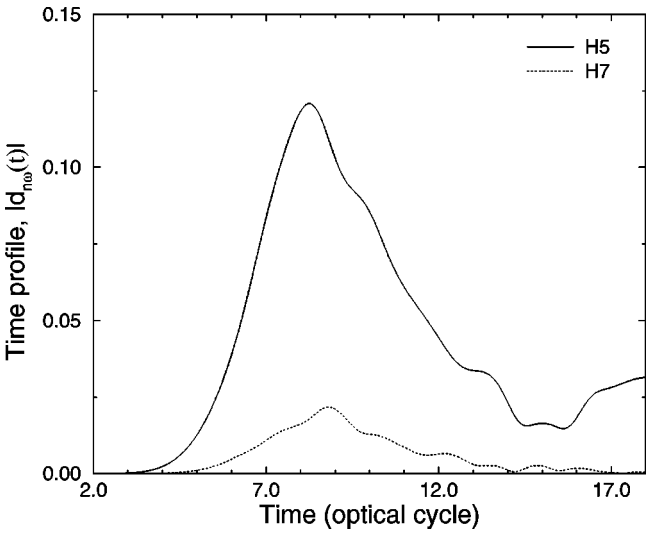

FIG. 5. The time profiles of the fifth and seventh harmonics of Na obtained from cross sections of the time-frequency spectrum in Fig. 4 at two different frequencies, 5ω and 7ω, respectively. Laser parameters are the same as those in Fig. 1.

B. Wavelet time-frequency analysis of the HHG spectrum of Na atoms in intense mid-ir laser pulses

To explore the origins of the HHG spectral fine structures, we perform a time-frequency analysis by means of the wavelet transform [7,12,32] of the induced dipole length (or dipole acceleration) moment,

$$A_\omega(t_0,\omega)=\int d(t)w_{t_0,\omega}(t)dt\equiv d_\omega(t_0), \tag{12}$$

with the wavelet kernel $w_{t_0,\omega}(t)=\sqrt{\omega}W(\omega(t-t_0))$. We used the Morlet wavelet [7,12]

$$W(x)=\frac{1}{\sqrt{\tau}}e^{ix}e^{-x^2/2\tau^2}. \tag{13}$$

Unlike the Gabor transform [12], the width of the window function in the wavelet transform varies as the frequency changes but the number of oscillations (proportional to τ) within the window is held constant. We have tested the dependence of $d_\omega(t_0)$ on the parameter τ by varying its value from 5 to 30. Although the absolute value of $d_\omega(t_0)$ depends somewhat on τ, the general temporal pattern does not change. In the following, we choose $\tau=15$.

Figure 4 shows the modulus of the time-frequency profiles of the induced dipole corresponding to the laser parameters used in Fig. 3, revealing striking details of the spectral and temporal structures. Several salient features are observed. (a) First, for the lowest few harmonics, the time profiles (at a given frequency) show a relatively smooth and continuous variation as a function of time, mimicking that of the driving laser pulse. [See also Fig. 5, where the time profiles are obtained from a cross section of the time-frequency profiles in Fig. 4 at a given frequency.] In this regime, the probability of absorbing N photons is roughly proportional to I^N, where I (laser intensity) is proportional to $E(t)^2$. (b) Second, for the harmonics in the plateau below the ionization threshold, the time profiles show some extended structure due to the effect of excited states. (c) Third, for those high harmonics in the plateau region well above the ionization threshold, the most prominent feature is the development of fast-burst time profiles. At a given time, we note that such bursts actually form a *continuous* frequency profile as seen in Fig. 4. This is clear evidence of the existence of *bremsstrahlung* radiation emitted by each recollision of the electron wave packet with the parent ion core. This supports the bremsstrahlung model of HHG [31] in the tunneling limit. In contrast, we find the (multiphoton-dominant) lowest harmonics form a continuous time profile at a given frequency. In the intermediate energy regime where both multiphoton and tunneling mechanisms contribute, the time-frequency profiles show a netlike structure as seen in Fig. 4. These features discussed here are qualitatively similar to those observed in the H-atom case [7].

Figure 6 depicts a representative time profile for near-cutoff harmonics ($H43$). As shown, it exhibits two bursts within each optical cycle. Each burst is due to the recollision of the electronic wave packet with the ion core. Also shown in Fig. 6 (vertical lines) are the electron returning times (with phase $\omega t=342°$ or $162°$) predicted by a quasiclassical model [33,34]. The agreement of the full quantum and quasiclassical prediction on the electron-ion recollision times indicates the validity of the quasiclassical model in the tunneling limit.

Next we consider the time-frequency profile of those harmonics in the plateau (below the cutoff). According to the quantum model (in the strong-field approximation) [35,36], when the electron return energy is below the cutoff, there exist two returning trajectories: the first (''short'') trajectory returns at a phase less than 342° (or 162°), and the second (''long'') trajectory returns at a phase (ωt) larger than 342° (or 162°). Such a feature is confirmed in Fig. 7 where we show a representative time profile for $H35$ in the plateau

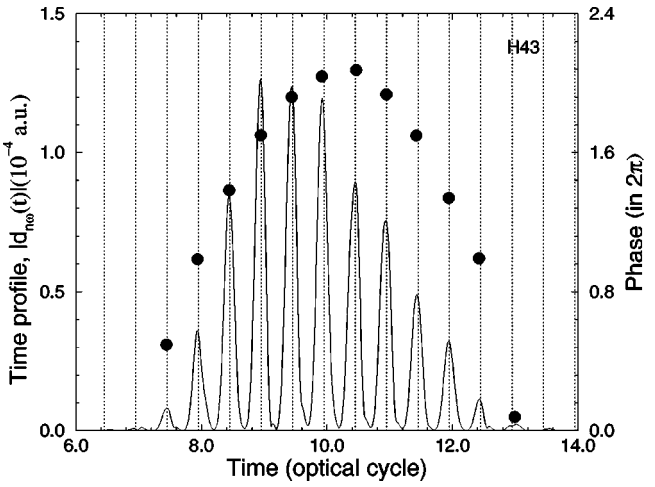

FIG. 6. The time profile of the 43rd harmonic of Na (near the cutoff). Laser parameters are the same as those in Fig. 1. The vertical dotted lines are the electron returning times predicted by the quasiclassical method. The black dots are the dynamical phases calculated from the wavelet transform of the induced dipole corresponding to each instant of the electron-ion core recollision.

below the cutoff. In this case, we see two bursts of light emission for each half optical cycle for the time duration corresponding to the central part of the laser pulse.

Also shown in Figs. 6 and 7 are the ''dynamical phases'' $\theta(t_q)$ (denoted by black dots) obtained from the wavelet transform of the induced dipole moment, corresponding to each instant (t_q) of electron-ion core recollision:

$$d_\omega(t_q)=|d_\omega(t_q)|e^{-iS(t_q)}, \tag{14}$$

where $S(t_q)=\omega t_q+\theta(t_q)$. Notice that the dynamical phase of the cutoff harmonics (Fig. 6) shows a time profile mimicking the laser-pulse shape. For the harmonics below the cutoff, we see in Fig. 7 that the ''long'' trajectory has stronger phase dependence on laser intensity than that of the

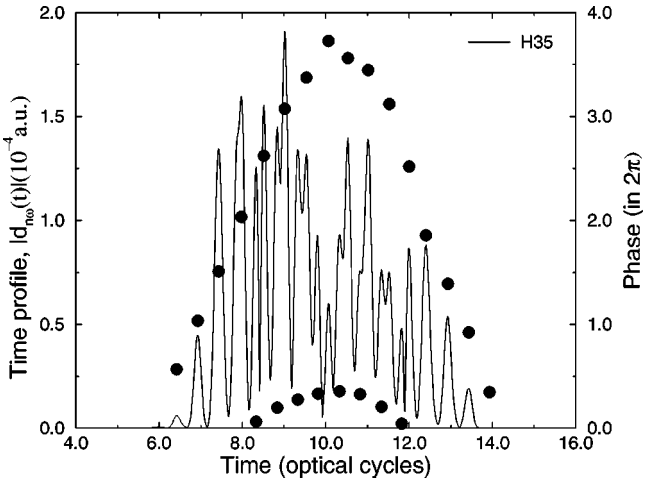

FIG. 7. The time profile of the 35th harmonic of Na (below the cutoff). Laser parameters are the same as those in Fig. 1. The black dots are the dynamical phases.

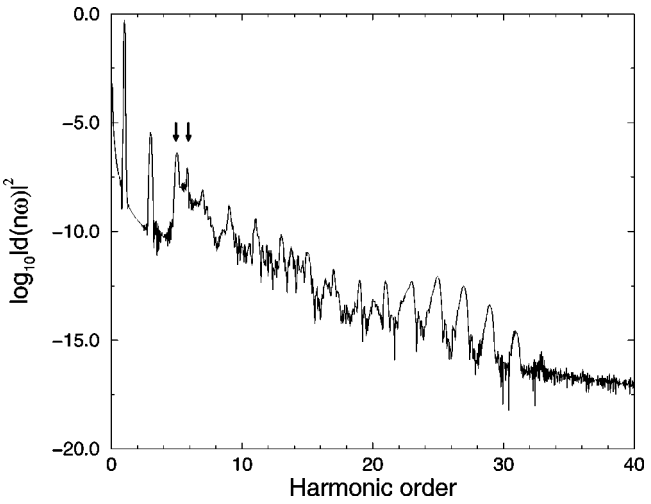

FIG. 8. The HHG power spectrum of Na in a mid-ir laser pulsed field with wavelength 3444 nm and intensity 1 TW/cm^2. The laser has a $\sin^2$ pulse shape and a duration of 20 optical cycles.

''short'' trajectory. Similar behavior was observed in our recent quantum studies of the H-atom [7] and molecular H_2 [10] systems.

C. Effect of multiphoton resonances on harmonic-generation processes

As indicated earlier in Sec. III A, a distinct feature of the alkali systems is the existence of strong coupling of the ground state with the first and other low-lying excited states, leading to enhancement of those harmonics below the ionization threshold. In this subsection, we investigate in more detail the effect of such bound-bound couplings on the harmonic generation processes and the consequence of such couplings for the time-frequency spectrum.

To explore the delicate effects of bound-bound couplings and multiphoton resonance, it is advantageous to study the HHG processes in a somewhat lower intensity case since the

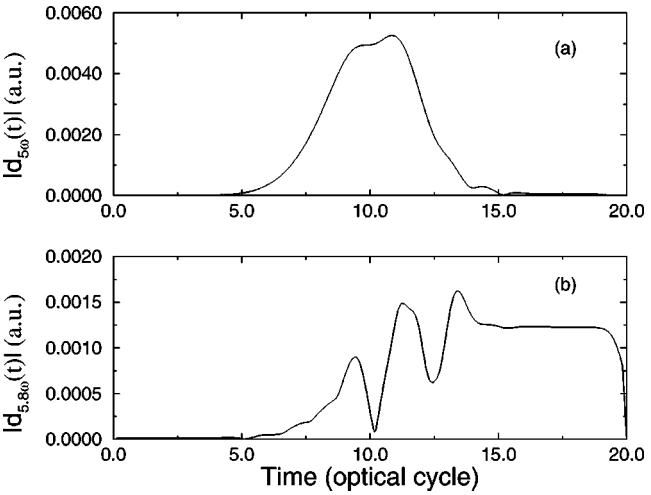

FIG. 9. The time profiles of (a) the fifth harmonic ($H5$) and (b) the subpeak $H5.8$ of Na. Laser parameters are the same as those in Fig. 8.

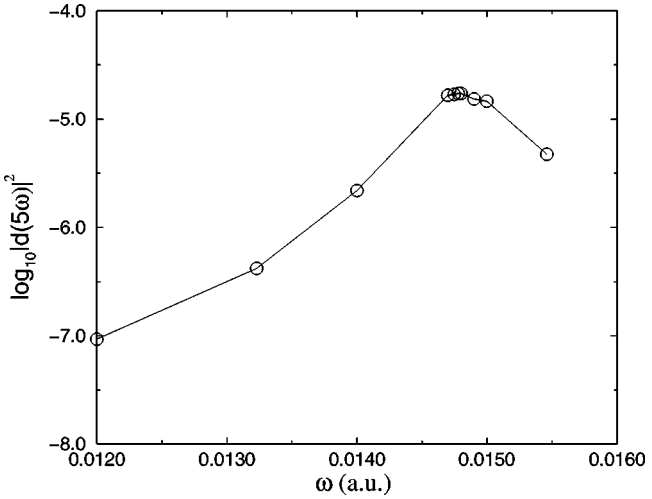

FIG. 10. The magnitude of the fifth harmonic of Na as a function of the laser frequency. The laser has a $\sin^2$ pulse shape with the peak intensity of 1 TW/cm^2 and the total pulse length is 20 optical cycles.

use of superstrong laser fields tends to wash out the detailed resonant fine structures [37]. For the mid-ir regime, the laser intensity used in recent alkali HHG experiments [3] is typically 1 TW/cm^2, which is in the medium-to-strong-field range. We thus adopt this laser intensity and use a laser frequency of 0.013 23 a.u. or 3444 nm, which is close to the five-photon $3s$-$3p$ resonance. It then takes about 14 photons to ionize the valence electron of a Na atom. The Keldysh parameter γ is 1.525 in this case, suggesting that the multiphoton mechanism plays an essential role in the HHG process. Figure 8 shows the HHG power spectrum of Na in the acceleration form. One of the most prominent features in Fig. 8 is the double-peak structure near the fifth harmonic where a multiphoton bound-bound resonance occurs.

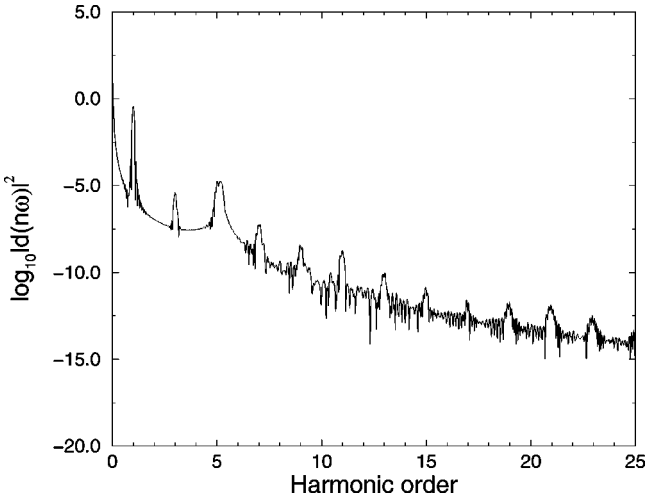

FIG. 11. The HHG power spectrum of Na in a mid-ir laser pulsed field with laser intensity 1 TW/cm^2, frequency 0.014 78 a.u., $\sin^2$ pulse shape, and 20 optical cycles duration. This laser frequency corresponds to the maximum enhancement of $H5$ in Fig. 10.

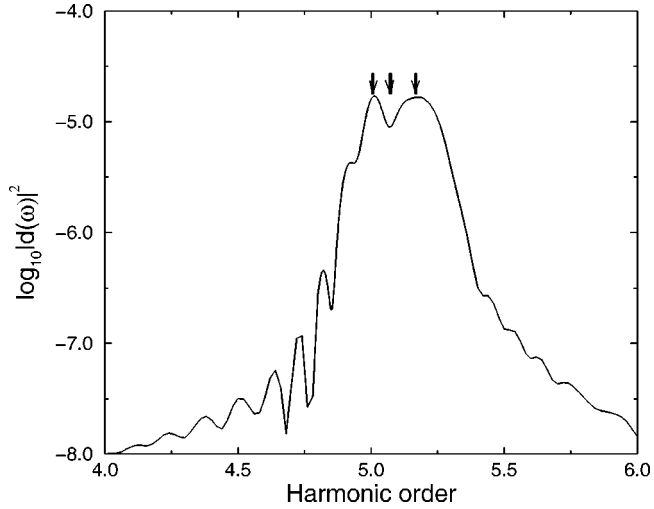

FIG. 12. The power spectrum of Na near the fifth harmonic regime, showing the detailed fine structure of the harmonic peak. Laser parameters are the same as those in Fig. 11.

Figures 9(a) and 9(b) show, respectively, the time profiles of the induced dipole (obtained from the wavelet transform) corresponding to the double-peak frequency positions in Fig. 8, namely, the fifth harmonic ($H5$) and the resonant-enhanced ($H5.8$) peaks. [Note that the $3p$-$3s$ (field-free) energy spacing amounts to about 5.8 photon energies in this case.] The time profiles for these two subpeaks are strikingly different, indicating that different origins are at work for their generation. The $H5$ time profile shows the typical smooth and continuous pattern of a nonresonant multiphoton-induced harmonic generation with some modification due to the existence of the nearby resonance (cf. Fig. 5). The $H5.8$ time profile for the multiphoton-resonance-induced peak is very different. Of special interest is the nearly flat time profile from 16 to 19 optical cycles. Such a flat plateau, which has not been reported before, is a ''signa-

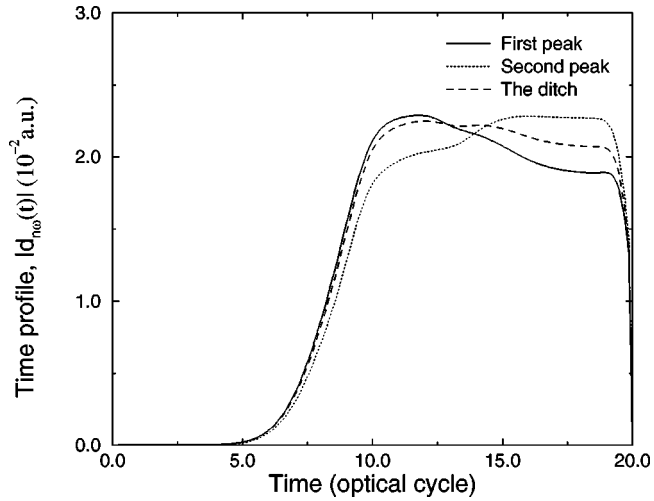

FIG. 13. The time profiles of Na, obtained by the wavelet transform of the induced dipole, corresponding to the three different frequency positions indicated by the arrows in Fig. 12. The laser parameters used are the same as those in Fig. 11.

ture'' of the existence of a multiphoton bound-bound resonance. Apparently the rapid Rabi flopping between the two-resonant $(3s,3p)$ levels has significantly extended the stimulated light emission duration well beyond the peak intensity regime to near the end of the laser pulse.

Finally, we study the enhancement of the fifth harmonic ($H5$) by tuning the laser frequency. Figure 10 shows the magnitude of $H5$ as a function of incident laser frequency. The laser intensity is fixed at 1 TW/cm^2. When $\omega = 0.014\,78$ a.u. (or $\lambda = 3083$ nm), the $H5$ emission intensity reaches a maximum and is more than two orders of magnitude larger than that at $\omega = 0.012$ a.u. The HHG power spectrum for this case is shown in Fig. 11. An enlarged power spectrum near the five-photon resonance region is depicted in Fig. 12. Again a double-peak structure is seen, though now the two subpeaks are much closer to each other with one of them due to $H5$ and the other broader peak due to the multiphoton resonance of $3s$-$3p$ transition occurring around $H5.2$. The time profiles of the induced dipole (obtained from the wavelet transform) at three different frequency positions (the first subpeak $H5$, the second subpeak $H5.2$, and the valley between the two subpeaks) are shown in Fig. 13. Although there is some difference in the detailed behavior of the time profiles, all the three profiles share the common feature of extended plateaulike stimulated emission pattern for the time period in the second half of the laser pulse. This is a special feature of the dipole time profiles associated with bound-bound multiphoton resonance.

In conclusion, we have presented in this paper an accurate 3D quantal calculation of the HHG power spectra of Na atoms in intense mid-ir laser pulsed fields. A detailed wavelet time-frequency analysis reveals detailed spectral and temporal fine structures and new insights into different harmonic generation mechanisms in different energy regimes.

ACKNOWLEDGMENTS

This work was partially supported by the U.S. Department of Energy, Office of Science, Office of Basic Energy Sciences, Division of Chemical Sciences. We are grateful to Kansas Center for Advanced Scientific Computing for the support of Origin2400 supercomputer time.

[1] A. L'Huillier *et al.*, Adv. At., Mol., Opt. Phys. **1**, 139 (1992).
[2] Z. Chang *et al.*, Phys. Rev. Lett. **79**, 2967 (1997); Ch. Spielmann *et al.*, Science **278**, 661 (1997); M. Schnürer *et al.*, Phys. Rev. Lett. **80**, 3236 (1998).
[3] B. Sheehy *et al.*, Phys. Rev. Lett. **83**, 5270 (1999); B. Sheehy *et al.*, in *Multiphoton Processes*, ICOMP VIII, edited by L.F. DiMauro, R.R. Freeman, and K.C. Kulander (American Institute of Physics, Melville, New York, 2000), p. 59.
[4] K.J. Schafer, M.B. Gaarde, K.C. Kulander, B. Sheehy, and L.F. DiMauro, in *Multiphoton Processes*, ICOMP VIII, edited by L.F. DiMauro, R.R. Freeman, and K.C. Kulander (American Institute of Physics, Melville, NY, 2000), p. 45.
[5] R. Trebino *et al.*, Rev. Sci. Instrum. **68**, 3277 (1997).
[6] X.M. Tong and S.I. Chu, Chem. Phys. **217**, 119 (1997).
[7] X.M. Tong and S.I. Chu, Phys. Rev. A **61**, 021802 (2000).
[8] X.M. Tong and S.I. Chu, Phys. Rev. A **57**, 452 (1998).
[9] X.M. Tong and S.I. Chu, Phys. Rev. A **58**, R2656 (1998).
[10] X. Chu and S.I. Chu, in *Multiphoton Processes* (Ref. [4]), p. 415; X. Chu and S.I. Chu, Phys. Rev. A (to be published).
[11] S.I. Chu and X.M. Tong, Chem. Phys. Lett. **294**, 31 (1998); X.M. Tong and S.I. Chu, Phys. Rev. A **61**, 031401 (2000).
[12] C.K. Chui, *An Introduction to Wavelets* (Academic Press, New York, 1992).
[13] G. Peach, *Atoms in Astrophysics*, edited by P.G. Burke *et al.* (Plenum, New York, 1983), p. 117.
[14] D.W. Norcross, J. Phys. B **4**, 1450 (1971).
[15] J.A. Kunc, J. Phys. B **32**, 607 (1999).
[16] C. Laughlin, J. Phys. B **11**, 1399 (1978).
[17] K. Butler and C. Mendoza, J. Phys. B **16**, L707 (1983).
[18] F. Rouet, R.J. Tweed, and J. Langlois, J. Phys. B **29**, 1767 (1996).
[19] W.M. Huo and Y-K. Kim, Chem. Phys. Lett. **319**, 576 (2000).
[20] C. Bottcher and A. Dalgarno, Chem. Phys. Lett. **36**, 137 (1975).
[21] C. Laughlin and G.A. Victor, Adv. At. Mol. Phys. **25**, 163 (1988).
[22] J.E. Hansen, C. Laughlin, H.W. van der Hart, and G. Verbockhaven, J. Phys. B **32**, 2099 (1999).
[23] W.R. Johnson, D. Kolb, and K-N. Huang, At. Data Nucl. Data Tables **28**, 333 (1983).
[24] E. Tiemann, H. Knöckel, and H. Richling, Z. Phys. D: At., Mol. Clusters **37**, 323 (1996).
[25] K.M. Jones, P.S. Julienne, P.D. Lett, D. Phillips, E. Tiesinga, and C.J. Williams, Europhys. Lett. **35**, 85 (1996).
[26] G. Yao and S.I. Chu, Chem. Phys. Lett. **204**, 381 (1993); J. Wang, S.I. Chu, and C. Laughlin, Phys. Rev. A **50**, 3208 (1994).
[27] C. Canuto, M.Y. Hussaini, A. Quarteroni, and T.A. Zang, *Spectral Methods in Fluid Dynamics* (Springer, Berlin, 1988).
[28] M.R. Hermann and J.A. Fleck, Jr., Phys. Rev. A **38**, 6000 (1988).
[29] T.F. Jiang and S.I. Chu, Phys. Rev. A **46**, 7322 (1992).
[30] L.V. Keldysh, Zh. Éksp. Teor. Fiz. **47**, 1945 (1964) [Sov. Phys. JETP **20**, 1307 (1965)].
[31] M. Protopapas *et al.*, Phys. Rev. A **53**, R2933 (1996).
[32] See, for example, P. Antoine, B. Piraux, and A. Maquet, Phys. Rev. A **51**, R1750 (1995); M. Graarde *et al.*, *ibid.* **57**, 4553 (1998).
[33] P.B. Corkum, Phys. Rev. Lett. **71**, 1994 (1993).
[34] K.C. Kulander, K.J. Schafer, and J.L. Krause, in *Super-Intense Laser-Atom Physics*, Vol. 316 of NATO Advanced Studied Institute, Series B, edited by P.B. Piraux *et al.* (Plenum, New York, 1993).
[35] M. Lewenstein *et al.*, Phys. Rev. A **49**, 2117 (1994).
[36] C. Kan *et al.*, Phys. Rev. A **52**, R4336 (1995).
[37] See, for example, S.I. Chu, Chem. Phys. Lett. **54**, 367 (1978).